Supporting Information

Pore-size-tuned host-guest interaction in Co-MOFs *via in situ* microcalorimetry: adsorption and magnetism

Chengfang Qiao,[a,b] Lin Sun,[a] Sheng Zhang,[a,c] Ping Liu,[b] Liangliang Chang,[b] Chunsheng Zhou,[b] Qing Wei,[a] Sanping Chen,*[a] Shengli Gao[a]

[a]*Key Laboratory of Synthetic and Natural Functional Molecule Chemistry of Ministry of Education, College of Chemistry and Materials Science, Northwest University, Xi'an 710127, P. R. China*

[b]*Shaanxi Key Laboratory of Comprehensive Utilization of Tailings Resources, College of Chemical Engineering and Modern Materials, Shangluo University, Shangluo 726000, P. R. China*

[c]*College of Chemistry and Chemical Engineering, Baoji University of Arts and Sciences, Baoji 721013, P. R. China*

Corresponding author: Prof. Sanping Chen

E-mail: sanpingchen@126.com

Table of contents Page

1. Experimental Section

Elemental analyses of C, H, and N were performed on a Vario EL III fully automated trace element analyzer. The FT-IR spectra were recorded on a Nicolet Magna 750 FT-IR spectrometer using KBr pellets in the range of 4000-400 cm^{-1}. Thermogravimetric analyses were investigated using a Netzsch STA 449C thermogravimetric analyzer. The gaseous products from the samples during heating under N_2 atmosphere were analyzed by an online FTIR (Bruker, Vertex70) with a 200 ml gas cell in the range of 4000-400 cm^{-1}. The phase purity of the bulk samples were verified by powder X-ray diffraction (PXRD) radiation (λ= 1.5406 Å), with a scan speed of 5° min^{-1} and a step size of 0.02° in 2θ. Inductively coupled plasma (ICP) analyses were performed on a Perkin–Elmer Optima 3300 DV ICP spectrometer. Magnetic measurements were performed in the temperature range 1.9 K-300 K, using a Quantum Design MPMS-XL-7 SQUID magnetometer on polycrystalline samples. The diamagnetic corrections for the compounds were estimated using Pascal's constants. The self-assembly processes were performed using a microcalorimeter of Tian-Calvet type (C80 from Setaram) in air atmosphere and then heated from 25 to 200 °C at a 0.5 °C min^{-1} heating rate. The heat capacities were measured using a Quantum Design PPMS in zero magnetic field. The adsorption heat was performed by using a RD496-III type microcalorimeter.[S1] The calorimetric constants at 295.15, 298.15, 301.15, 304.15, and 307.15 K were determined, by the Joule effect, to be 63.799 ± 0.025, 63.901 ± 0.030, 64.000 ± 0.026, 64.075 ± 0.038, and 64.203 ± 0.043 μV · mW^{-1}, respectively. The enthalpy of the dissolution of KCl (spectral purity) in deionized water was measured to be 17.238 ± 0.048 kJ · mol^{-1}, which is in good agreement with the value of 17.241 ± 0.018 kJ · mol^{-1} from ref.[S2] The accuracy is 0.02%, and the precision is 0.3%, which indicates that the calorimetric system is accurate and reliable.

1.1 Synthesis

1.1.1 Synthesis of $[Co_3(OH)_2(L)_2]\cdot 4H_2O$ (1•$4H_2O$)

A mixture of benzotriazole-5-carboxylic acid (H_2L; 0.2 mmol, 0.048 g), $CoSO_4\cdot 6H_2O$ (0.4 mmol, 0.116 g), N,N-dimethylformamide (5 mL), and H_2O (3 mL) was sealed in a 15-mL Teflon-lined stainless container, which was heated to 150 °C and kept at that temperature for 3 days. After cooling to room temperature at a rate of 3 °C min^{-1}, purple crystals were recovered in 48% yield by filtration. The bulk phase purity was confirmed by PXRD. Elemental analysis (%) calcd.

for $C_{14}H_{16}Co_3N_6O_{10}$ (M_r = 605.12): C 27.77, H 2.67, N 13.89; found: C 27.32, H 2.61, N 14.13. IR (cm^{-1}): 3438 (s), 2931 (w), 2652 (w), 1638 (s), 1541 (m), 1409 (s), 1271 (w), 1069 (m), 792 (m).

1.1.2 Synthesis of $[Co_3(OH)_2(L)_2]\cdot 2DMF$ (2•2DMF)

An identical procedure with **1•4H_2O** was followed to prepare **2•2DMF** except for the temperature. The same mixture was heated at 180 °C for 3 days to generate **2•2DMF**. Red crystals were recovered in 42% yield by filtration. The bulk phase purity was confirmed by PXRD. Elemental analysis (%) calcd. for $C_{20}H_{22}Co_3N_8O_8$ (M_r = 679.25): C 35.37, H 3.26, N 16.50; found: C 35.42, H 3.74, N 16.41. IR (cm^{-1}): 3462 (s), 2912 (w), 2665 (w), 1645 (s), 1543 (m), 1411 (s), 1262 (w), 1061 (m), 783 (m).

1.1.3 Synthesis of $[Co_3(OH)_2(L)_2]\cdot EtOH$ (1•EtOH)

The dehydrated **1•4H_2O** samples were immersed in 20 mL of ethanol, which was replaced with fresh ethanol every 3 h for 1 week, thus ensuring a complete incorporation of ethanol. The final products were separated by filtration and dried under ambient temperature. Dark-violet crystals of **1·EtOH** was recovered. The bulk phase purity was confirmed by PXRD. Elemental analysis (%) calcd. for $C_{16}H_{14}Co_3N_6O_7$ (M_r = 579.12): C 33.18, H 2.44, N 14.51; found: C 33.72, H 2.92, N 14.14. IR (cm^{-1}): 3428 (s), 3194 (s), 2352 (w), 1633 (s), 1548 (m), 1400 (s), 1276 (w), 1182 (m), 786 (m).

1.2. X-ray structure determination

Single-crystal X-ray diffraction data for all compounds were collected on a Bruker SMART APEXII CCD diffractometer, equipped with graphite-monochromatized Mo Kα radiation (λ = 0.71073 Å) using ω and φ scan mode. The data integration and reduction were processed with SAINT software. Absorption correction based on multi-scan was performed using the SADABS program.[S3] The structures were solved by direct methods and refined with full-matrix least-squares refinements based on F^2 using SHELXS-97 and SHELXL-97.[S4] All non-hydrogen atoms were refined anisotropically. Hydrogen atoms were fixed geometrically at calculated distances and allowed to ride on the parent non-hydrogen atoms, whereas those of free ethanol solvent molecules and water molecules were not treated during the structural refinements due to disorder. A summary of the crystallographic data and data collection, refinement parameters are listed in Table S1. Selected bond distances and angles are given in Tables S2. Hydrogen-bonding

interactions are shown in Table S3.

1.3. Thermodynamic process for solvothermal synthesis mechanism and adsorption process

The self-assembly process was measured with a Setaram C80 calorimeter equipped with a membrane mixing cell. The temperature accuracy of the calorimeter was 0.1 K. The calorimeter was calibrated by using two well-known recommended chemical reference systems: cyclohexane−hexane and methanol−water. The calibration procedure indicated for this type of equipment was utilized. The cyclohexane−hexanebinary system was used to determine the sensitivity of the calorimeter, and the methanol−water binary system was used to check the accuracy of the calibration. The average accuracy of the calorimeter was found to be 2.6%.[S5]

The reaction solvent (5 mL) was put into a stainless steel sample cell in a 15 mL container.[S6] At equilibrium, the proper amounts sample of Co-MOFs (20-22 mg) were pushed down simultaneously. As a result, the crystals and solvent were mixed at 298.15 K, and the thermogram of the crystalline-state-liquid guest exchange was recorded. The enthalpy of the process was detected by a RD496-III type microcalorimeter.

1.4 Calculation of sorption heat for CO_2 uptake using Virial 2 model

$$\ln P = \ln N + 1/T\sum_{i=0}^{m} a_i N^i + \sum_{i=0}^{n} b_i N^i \qquad\qquad Q_{\mathrm{st}} = -R\sum_{i=0}^{m} a_i N^i$$

The virial expression above was used to fit the combined isotherm data for **2•2DMF** at 273.15 and 298 K, where P is the pressure, N is the adsorbed amount, T is the temperature, a_i and b_i are virial coefficients, and m and N are the number of coefficients used to describe the isotherms. Q_{st} is the coverage-dependent enthalpy of adsorption and R is the universal gas constant.

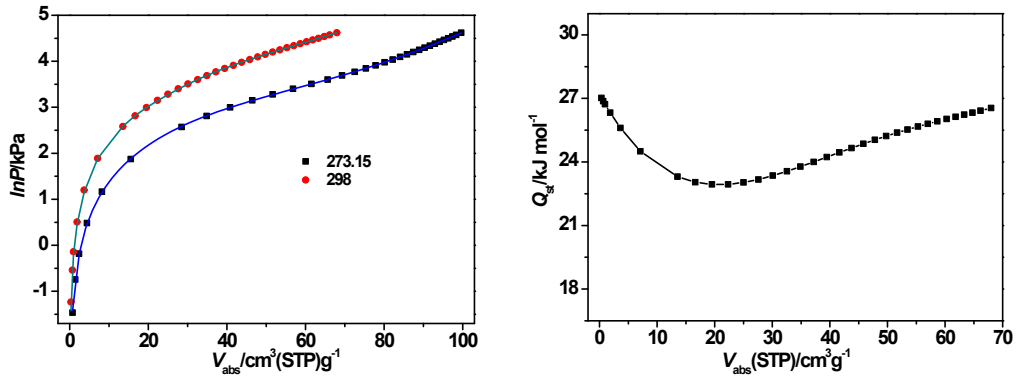

(a) (b)

Fig. S1. (a) CO_2 adsorption isotherms for desolvated compound of **2•2DMF** with fitting by Virial 2 model. Fitting results: a0 = -3269.68437, a1 = 60.1094, a2 = -2.28855, a3 =0.0311, b0 = 10.85946, b1= -0.19686, b2= 0.00785, b3= -0.00011, Chi^2 = 0.0008, R^2 = 0.99997. (b) CO_2 adsorption heat calculated according to the virial equation.

1.5 Cr(VI) adsorption

1.5.1 Batch adsorption experiments

Potassium chromate (K_2CrO_4, 373.7 mg) was dissolved in 100 mL of deionized water to prepare a Cr(VI) solution with the concentration of 1000 mg L^{-1}. The other solutions were obtained by appropriate dilution of the stock solution. The amount of solid adsorbent was adjusted to be 10 mg in all experiments. The mixture was then centrifuged at 12000 rpm for 5 min, and the concentration of remaining Cr(VI) was determined by ICP analysis.

1.5.2 Effect of pH

Evaluation of pH effects on Cr(VI) adsorption was done at a pH range of 1.0−10.0. The adjustment of pH was performed by adding either 0.1 M HCl or 0.1 M NaOH while the initial concentration of Cr(VI) was kept at 30 mg L^{-1} for all samples to 100 mL containing 10 mg of **2·2DMF** at 298K. The Cr(VI) adsorption efficiency (% adsorption) was obtained using eq 1,

$$\%\ \text{adsorption} = \left(\frac{C_0 - C_e}{C_0}\right) \times 100 \qquad (1)$$

where C_o and C_e are the initial and the equilibrium Cr(VI) concentrations (mg L^{-1}), respectively.

1.5.3 Kinetics for the Cr(VI) adsorption

The samples were prepared by adding a fixed concentration of Cr(VI) (30 mg L^{-1}) to 50 mL conical flasks containing 10 mg of **2·2DMF** at 298 K. The adsorption process was stopped at different times from 1 to 120 min. Then, the mixture was centrifuged at 12000 rpm for 5 min and sampled for ICP analysis. The amount of Cr(VI) adsorbed was calculated using eq 2, and the

experimental data were fitted with a pseudo-second-order kinetic model using the following eq3:

$$q_t = \frac{(C_0 - C_t)V}{m} \tag{2}$$

$$\frac{t}{q_t} = \frac{1}{k_{ad} q_e^{\,2}} + \frac{t}{q_e} \tag{3}$$

where q_t and C_t are the amount of Cr(VI) adsorbed per unit mass of adsorbent (mg g^{-1}) and the Cr(VI) concentration (mg $L^{-1)}$ at time t (min), respectively; m is the adsorbent mass (g), and V is the volume (L) of the sample, k_{ad} (g mg^{-1} min^{-1}) is the rate constant of adsorption, q_e (mg g^{-1}) is the adsorption capacity at equilibrium.

1.5.4 Adsorption isotherms and thermodynamic evaluations

To study the adsorption isotherm, 50 mL of Cr(VI) aqueous solution (the initial Cr(VI) concentrations varying from 5 to 100 mg L^{-1}) was poured into a Falcon conical tube with 10.0 mg of the MOFs and shaken for 2 h at 298 K. The mixture was then centrifuged at 12000 rpm for 5 min, and the concentration of remaining Cr(VI) was determined by ICP analysis. The equilibrium adsorption capacity was determined using eq 4, and the experimental Cr(VI) uptake data were best fitted using a Freundlich model eq 5:

$$q_e = \frac{(C_0 - C_e)V}{m} \tag{4}$$

$$\lg q_e = \lg k_f + \frac{1}{n} \lg C_e \tag{5}$$

where q_e is the equilibrium amount of Cr(VI) adsorbed per unit mass of adsorbent (mg g^{-1}) and C_0 and C_e are initial and equilibrium concentrations of Cr(IV), where k_f is the binding energy constant ($mg^{1-(1/n)} \cdot L^{1/n}/g$) and n is the Freundlich exponent, respectively.

2. References

[S1] Ji M. , M.Y. Liu, S.L. Gao, *Instrum. Sci. Technol.* **2001**, *29*, 53-57.

[S2] V. K. J. Marthada, *Res. NBS Standards* **1980**, *85*, 467-470.

[S3] G. M. Sheldrick, SADABS, Program for Empirical Absorption Correction; University of Göttingen, Göttingen, Germany, **1996**.

[S4] G. M. Sheldrick, SHELXTL; Bruker Analytical X-ray Instruments Inc., Madison, WI, **1998**.

[S5] H. Laavi, J. P. Pokki, P. Uusi-Kyyny, Y. Kim, V. Alopaeus, *J. Chem. Eng. Data*, **2013**, 58, 943−950.

[S6] S. L.Gao, Y. Fang, S. P. Chen, *Acta Chim. Sin.* **2002**, *6*0, 2220-2224.

[S7] X. M. Zhang, Z. M. Hao, W. X. Zhang, and X. M. Chen, *Angew. Chem. Int. Ed*., 2007, 46, 3456 –3459.

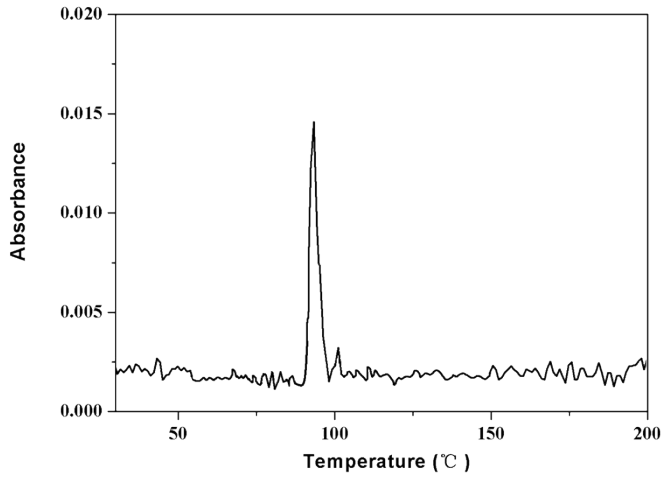

(a)

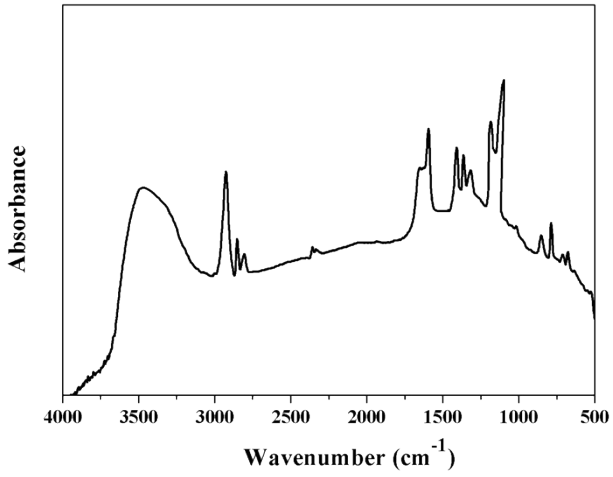

(b)

Fig. S2 (a) The corresponding Gram–Schmidt signal of **1·EtOH**. (b) Gas phase IR spectra corresponding to the maximum of the Gram–Schmidt signal in **1·EtOH**.

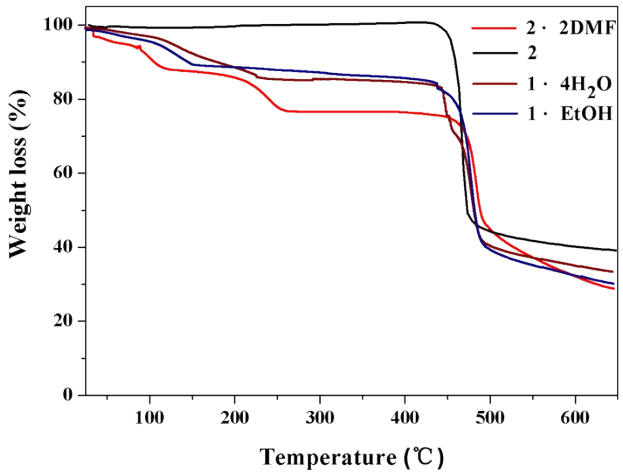

Fig. S3 TG curves for **2·2DMF**, the desolvated compound of **2·2DMF**, **1·4H$_2$O**, and **1·EtOH** under a nitrogen atmosphere.

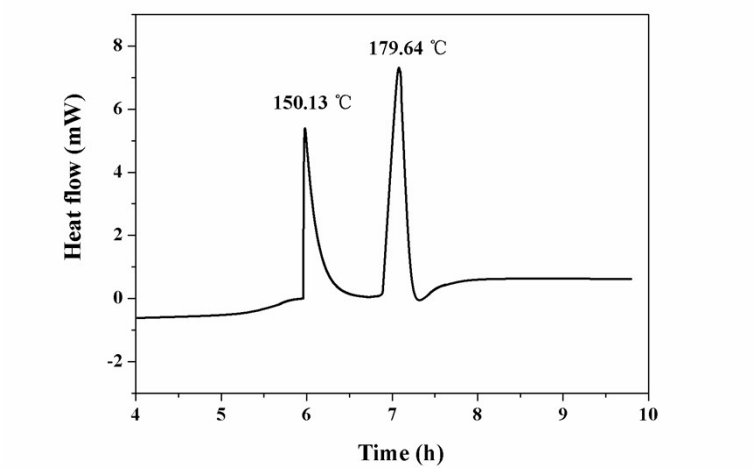

Fig. S4 Plot of heat flow *vs* time of the reaction process.

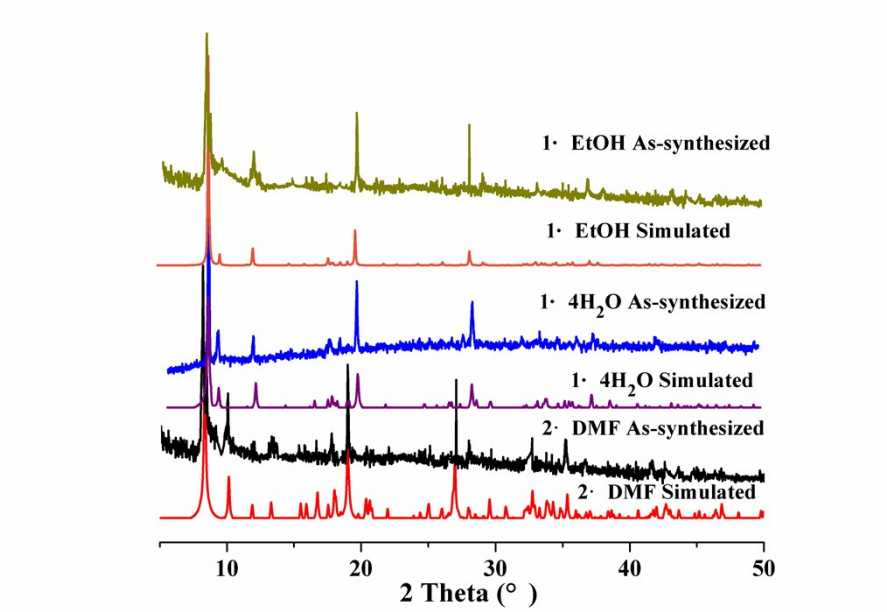

Fig. S5 Powder XRD patterns of **2·2DMF**, **1·4H$_2$O**, **1·EtOH** and their simulated ones.

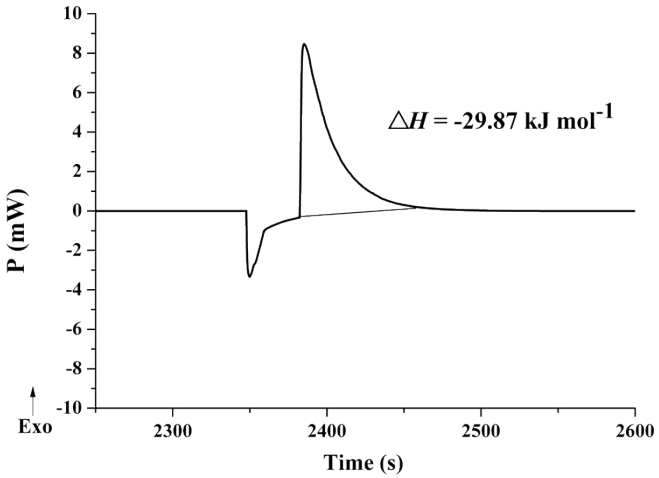

(a)

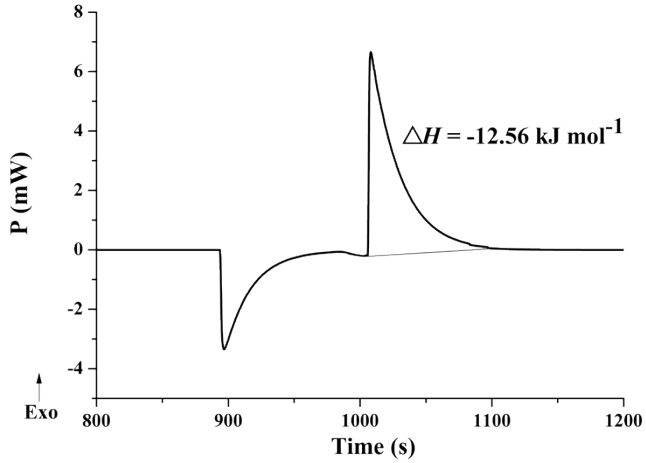

(b)

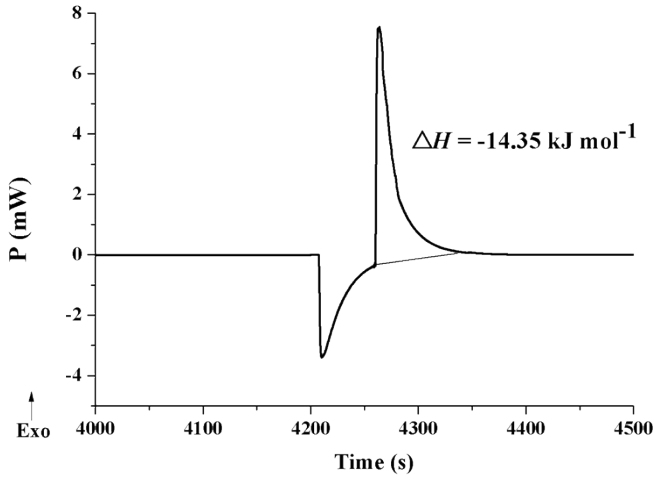

(c)

Fig. S6 Variation of heat-flow as a function of time: (a) desolvated compound of **2·2DMF** and DMF system, (b) dehydrated compound of **1·4H$_2$O** and H_2O system, (c) desolvated compound of **1·EtOH** and ethanol system.

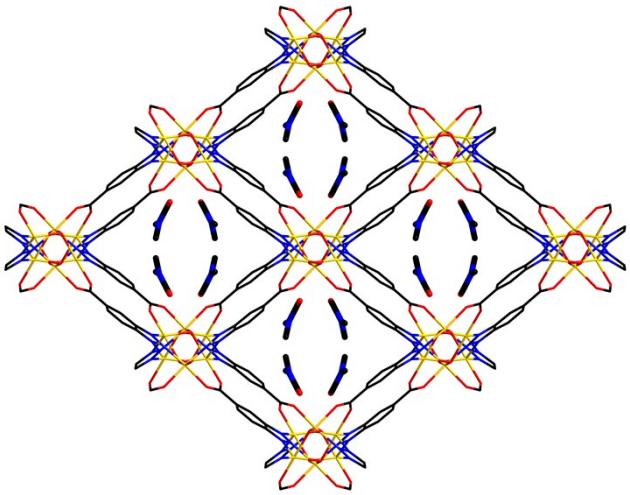

Fig. S7 View of the 3D framework of **2•2DMF** shown in Wires/Sticks mode along the *c*-axis. All H atoms are omitted for clarity.

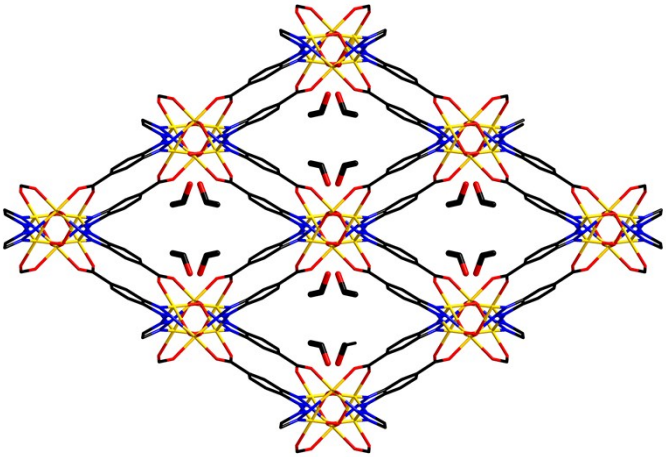

Fig. S8 View of the 3D framework of **1•EtOH** shown in Wires/Sticks mode along the *c*-axis. All H atoms are omitted for clarity.

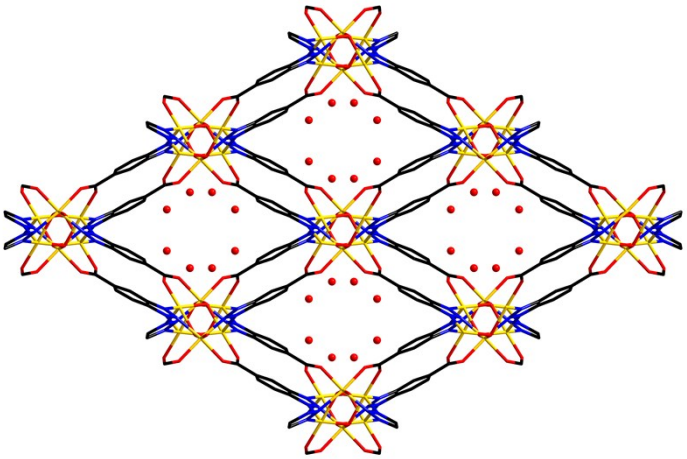

Fig. S9 View of the 3D framework of **1•4H_2O** shown in Wires/Sticks mode along the *c*-axis. All H atoms are omitted for clarity.

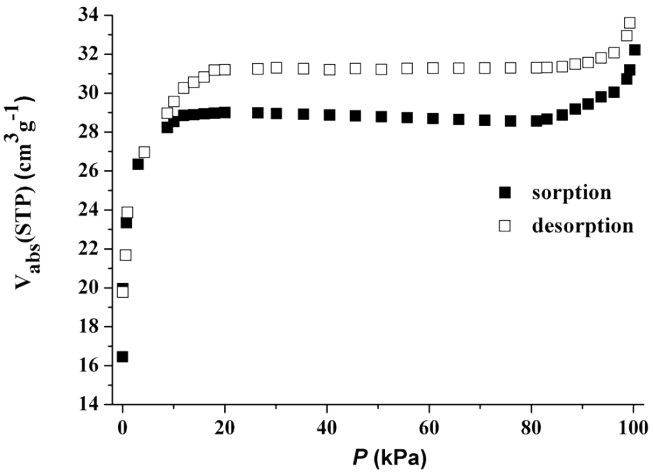

Fig. S10 N_2 sorption isotherm (77 K) for the desolvated samples of **1·4H_2O**.

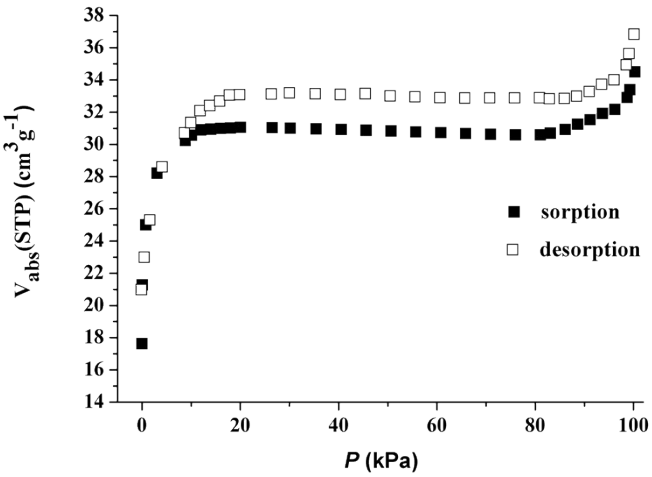

Fig. S11 N_2 sorption isotherm (77 K) for the desolvated samples of **1·EtOH**.

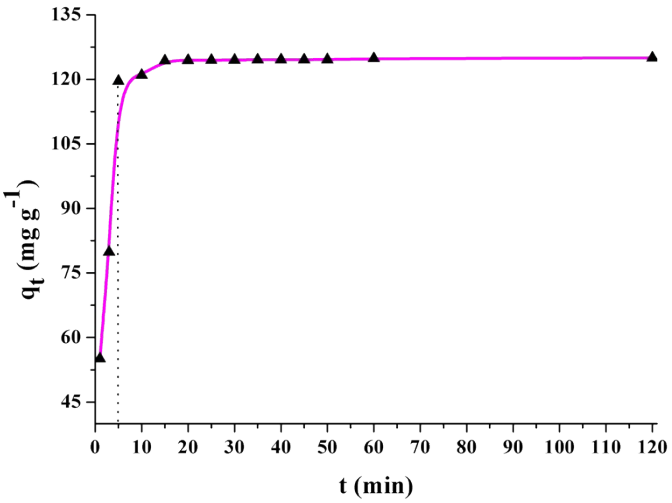

Fig. S12 Effect of time on the Cr(VI) adsorption by 10 mg of **2·2DMF** with initial concentration of 30 mg L^{-1}. q_t represents the amount of Cr(VI) adsorbed at different times.

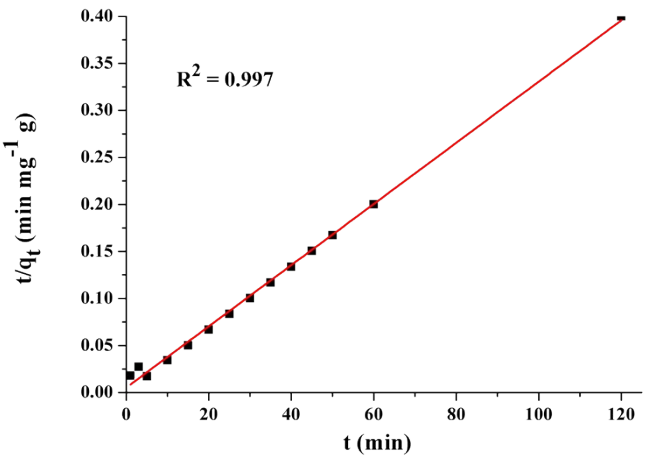

Fig. S13 Linear pseudo-second-order kinetic model for adsorption of Cr(VI) on **2·2DMF** (Initial Cr(VI) concentration: 30 mg/L; amount of adsorbent: 10 mg; sample volume: 50 mL; pH: 5.6; T: 298 K).

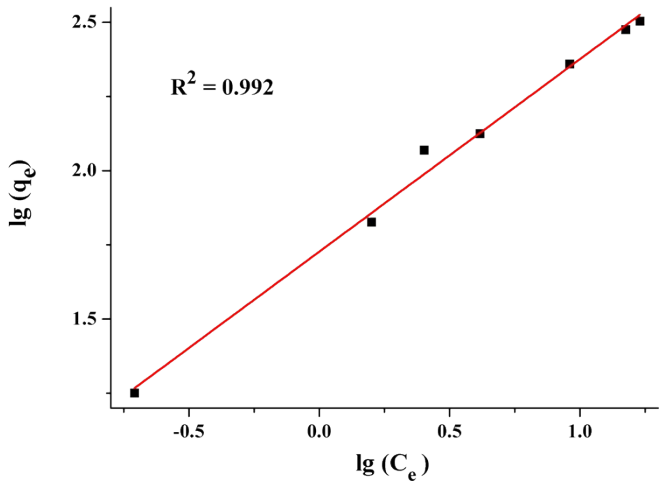

Fig. S14 Freundlich linear plot; amount of adsorbent: 10 mg; contact time: 2 hours; sample volume: 50 mL; pH: 5.6; T: 298 K. (y = 0.64x + 1.72)

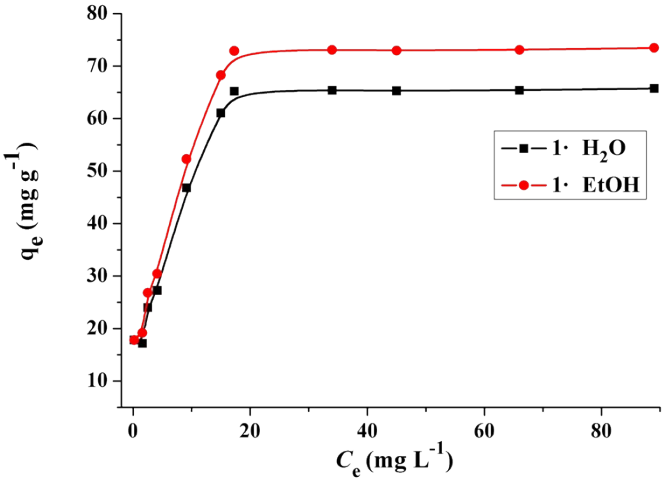

Fig. S15 Effect of initial Cr(VI) concentration on adsorption by 10 mg of **1·EtOH** and **1·4H$_2$O**; C_e, equilibrium concentration of adsorbate; q_e, the adsorbed amount of Cr(VI).

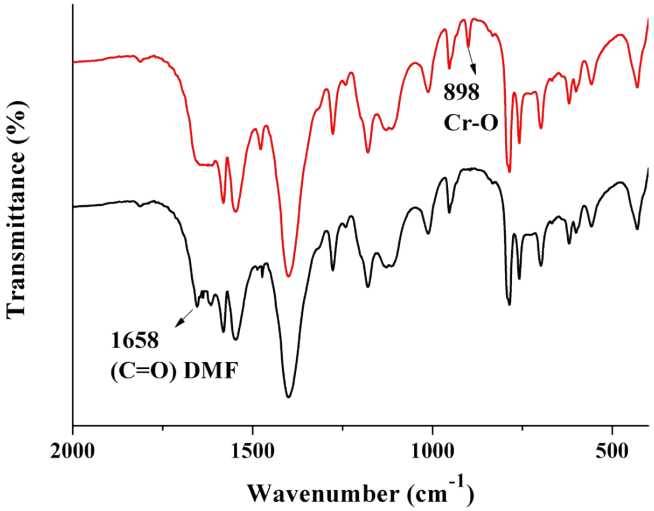

Fig. S16 FT-IR spectra of as-synthesized **2·2DMF** (black line) andCr(VI)-adsorbed **2·2DMF** (red line).

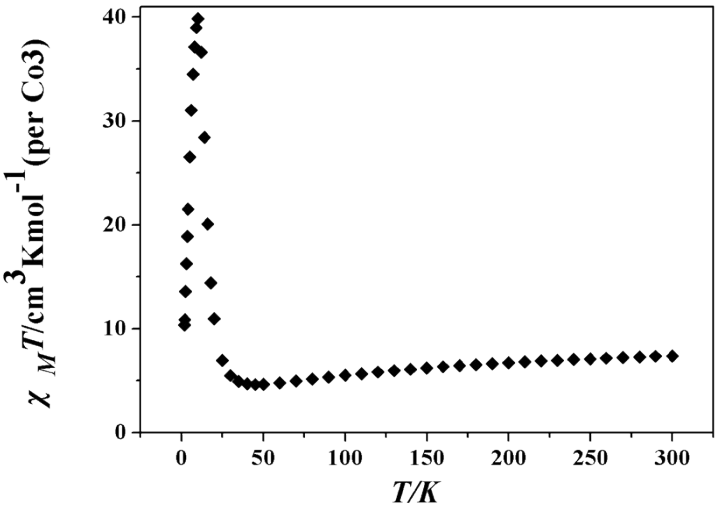

Fig. S17 Temperature dependence of $\chi_M T$ for **2•2DMF** under an applied dc fields of 1 kOe.

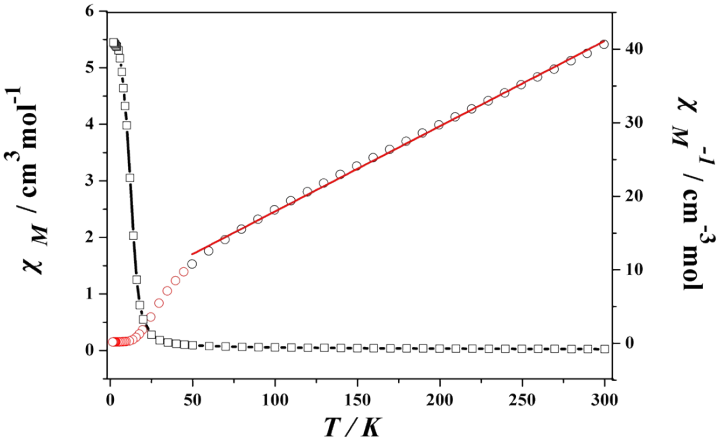

Fig. **S18** The thermal dependence of χ_M and χ_M^{-1} for **2•2DMF**. The red solid lines correspond to the best-fit curves (y=6.30853+0.11594x).

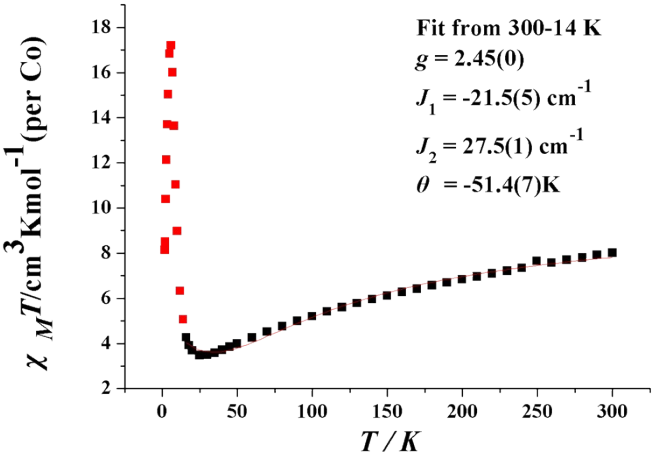

Fig. **S19** The measured (black cycle) and fited (red line) $\chi_M T$ versus T curve of **2·2DMF** per Co^{II}. The fitting was conducted by using an alternating 1-D Heisenberg chain (S= 3/2) model with

orbital contribution item. The used formula is the follows [S7]:

$$\chi = \frac{C}{(1-u_1^2u_2)^2}\{(1-u_1^4u_2^2)+4u_1(1-u_1^2u_2^2)+2u_2(1+u_1)^2(1-u_1^2)+2u_1^2(1-u_2^2)\}$$

$$u_i = \coth(\frac{J_iS(S+1)}{kT}) - \frac{kT}{J_iS(S+1)} \quad (i = 1, 2)$$

$$C = \frac{Ng^2S(S+1)\mu_B^2}{3k(T-\theta)}$$

$S = 3/2$ (Cobalt(II))

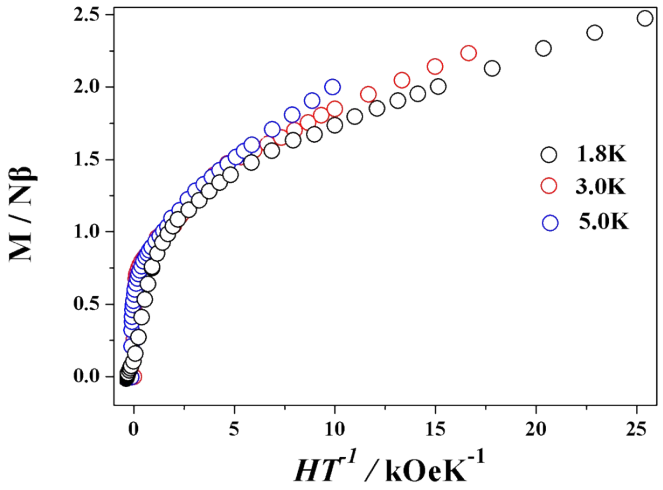

Fig. **S20** Field dependence of magnetization plot for **2·2DMF** at 1.8 K, 3.0K and 5.0K.

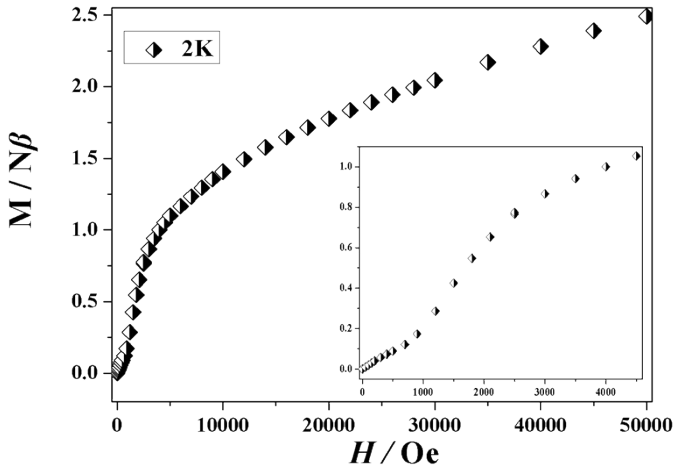

Fig. S21 Magnetization *vs* field plot of **2·2DMF** at 1.8 K. Inset: magnetization versus *H* plots in fields of 0−5 kOe.

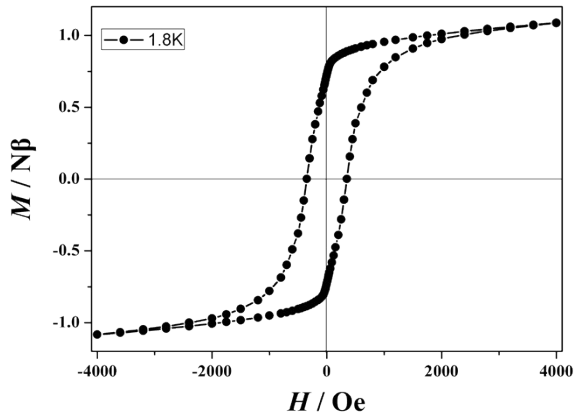

Fig. S22 Magnetic hysteresis loop of **2·2DMF** recorded at 1.8 K.

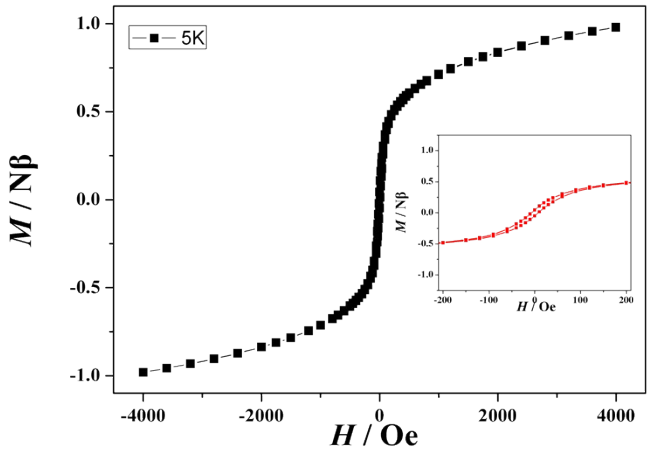

Fig. S23 Magnetic hysteresis loop of **2·2DMF** recorded at 5 K.

The magnetic susceptibility data were described by the modified Debye functions:

$$\chi'(\omega) = \chi_S + (\chi_T - \chi_S)\frac{1+(\omega\tau)^{1-\alpha}\sin(\frac{\pi}{2}\alpha)}{1+2(\omega\tau)^{1-\alpha}\sin(\frac{\pi}{2}\alpha)+(\omega\tau)^{(2-2\alpha)}}$$

$$\chi''(\omega) = (\chi_T - \chi_S)\frac{(\omega\tau)^{1-\alpha}\cos(\frac{\pi}{2}\alpha)}{1+2(\omega\tau)^{1-\alpha}\sin(\frac{\pi}{2}\alpha)+(\omega\tau)^{(2-2\alpha)}}$$

Table S1. Relaxation fitting parameters from Least-Squares Fitting of $\chi(\omega)$ data of **2·2DMF**.

T(K)	$\Delta\chi_1$ (cm^3mol^{-1})	$\Delta\chi_2$ (cm^3mol^{-1})	α_1	τ_1(s)
2.5	3.903	1.406	0.628	0.0226
2.6	4.010	1.610	0.596	0.0110
2.7	4.258	1.858	0.587	0.00589

2.8	4.447	2.047	0.576	0.00313
2.9	4.544	2.144	0.561	0.00166
3.0	4.646	2.247	0.534	0.0009215
3.1	4.852	2.352	0.517	0.000472
3.2	5.093	2.493	0.489	0.000261
3.3	5.172	2.772	0.432	0.000149
3.4	5.231	2.831	0.414	0.0000865

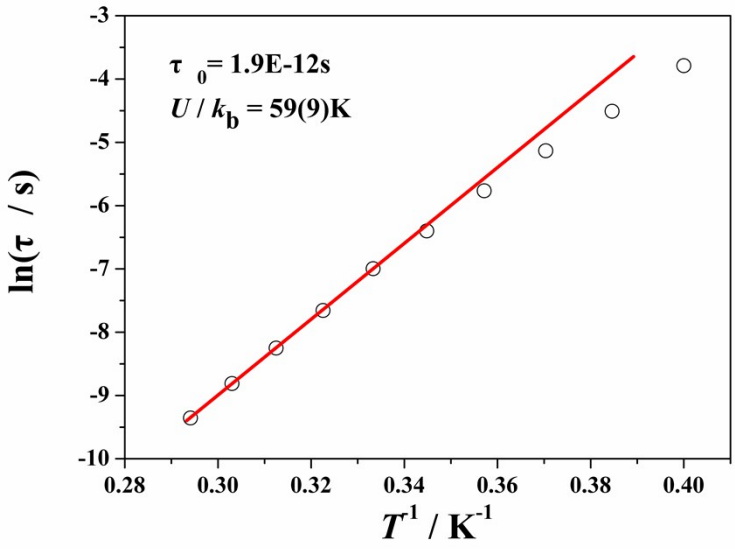

Fig. S24 Magnetization relaxation time, *lnτ vs.* T^{-1} plot under 0 Oe dc field for **2·2DMF**. The solid line is fitted with the Arrhenius law.

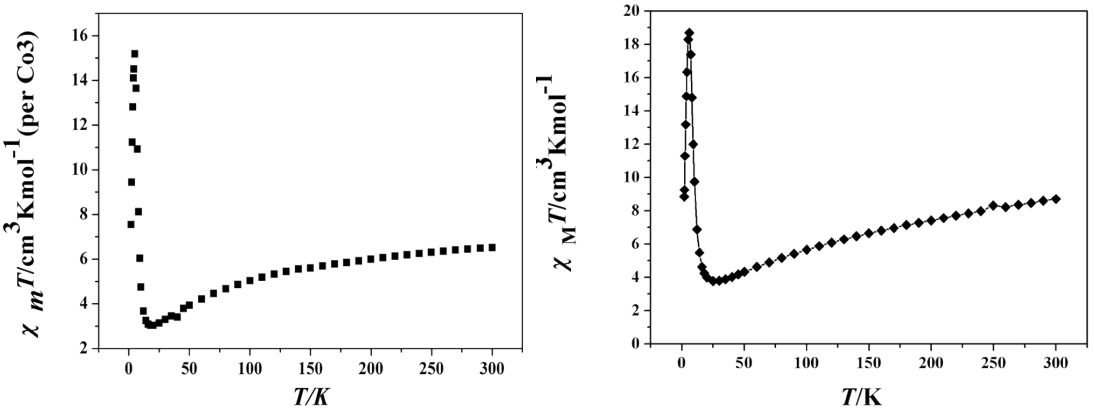

Fig. **S25** $\chi_M T$ vs T plot for desolvated compound of **2·2DMF** at 1000 Oe (left). $\chi_M T$ vs T plot for **1•EtOH** at 1000 Oe (right).

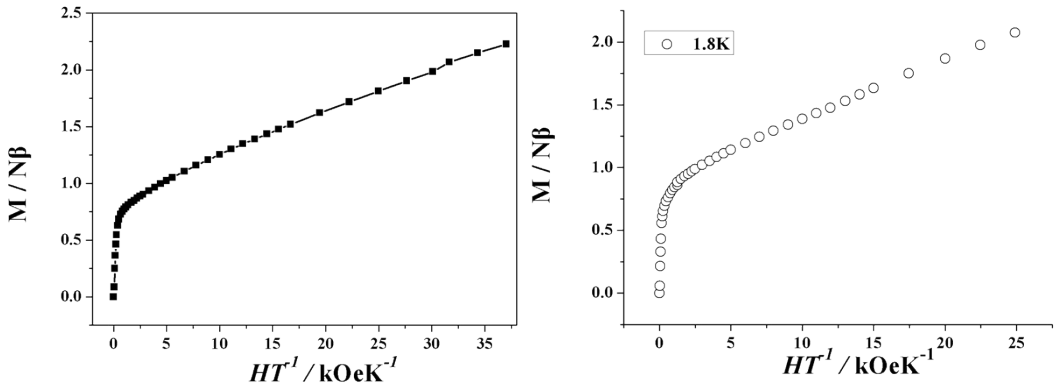

Fig. **S26** Field dependence of magnetization plot for desolvated compound of **2·2DMF** at 1.8 K (left). Field dependence of magnetization plot for **1•EtOH** at 1.8 K (right).

Table S2. Crystal data and refinement parameters for the title compounds.

Compound	**2•2DMF**	**1•4H_2O**	**1•EtOH**
Empirical formula	$C_{20}H_{22}Co_3N_8O_8$	$C_{14}H_{16}Co_3N_6O_{10}$	$C_{16}H_{14}Co_3N_6O_7$
Formula weight	679.25	605.12	579.12
Crystal system	Monoclinic	Monoclinic	Monoclinic
Space group	*C*2/*c*	*C*2/*c*	*C*2/*c*
a/Å	**17.518(9)**	**18.373(9)**	**18.280(3)**
b/Å	**13.309(9)**	**11.523(6)**	**11.9163(18)**
c/Å	**11.181(6)**	**11.034(5)**	**11.0923(17)**
α/º	90	90	90
β/º	95.873(15)	94.251(9)	94.040(2)
γ/º	90	90	90
V/Å ^{3}	2593(3)	2330(2)	2410.3(6)
Z	4	4	4
D_c/(g·cm^{-3})	1.740	1.725	1.596
T (K)	296(2)	200(2)	296(2)
F(000)	1372	1212	1156
Absorption coefficient/mm^{-1}	1.958	2.171	2.086
Reflections collected/unique	6193 / 2282	5208 / 1961	6359 / 2387
R(int)	0.1293	0.0494	0.0472
GOF	1.021	1.062	1.054
R_1[a] [$I>2\sigma(I)$]	0.0971	0.0794	0.0555
wR_2[b] (all data)	0.2718	0.2833	0.1819
CCDC number	1496242	1496243	1496244

[a] $R_1 = \sum||F_o| - |F_c||/\sum|F_o|$

[b] $wR_2 = [\sum w(F_o^2 - F_c^2)^2/\sum w(F_o^2)^2]^{1/2}$

Table S3. Selected bond lengths (Å) and bond angles (°) for compounds.

2•2DMF					
Bond lengths					
Co(1)-O(1)#1	2.078(6)	Co(1)-O(3)	2.080(5)	Co(1)-N(2)	2.146(7)
Co(2)-O(3)#4	2.012(6)	Co(2)-O(3)	2.157(6)	Co(2)-O(2)#5	2.018(6)
Co(2)-N(3)	2.082(7)	Co(2)-N(1)#6	2.069(7)		
Bond angles					
O(3)-Co(1)-N(2)	83.1(2)	O(1)#2-Co(1)-N(2)	86.0(3)	O(3)#3-Co(1)-N(2)	89.7(2)
O(1)#1-Co(1)-O(1)#2	89.8(4)	O(1)#1-Co(1)-O(3)	93.0(2)	O(1)#2-Co(1)-O(3)	94.8(2)
N(2)-Co(1)-N(2)#3	98.4(4)	O(3)-Co(1)-O(3)#3	169.0(3)	O(1)#1-Co(1)-N(2)	174.0(2)
O(3)#4-Co(2)-O(3)	78.9(2)	O(2)#5-Co(2)-N(1)#6	92.1(3)	O(3)#4-Co(2)-O(2)#5	101.7(2)
N(3)-Co(2)-O(3)	86.9(2)	O(2)#5-Co(2)-N(3)	92.9(3)	N(1)#6-Co(2)-N(3)	121.9(3)
N(1)#6-Co(2)-O(3)	87.4(2)	O(3)#4-Co(2)-N(1)#6	94.7(2)	O(3)#4-Co(2)-N(3)	140.1(2)
O(2)#5-Co(2)-O(3)	179.3(2)	Co(2)#4-O(3)-Co(1)	106.3(2)	Co(2)#4-O(3)-Co(2)	101.1(2)
Co(1)-O(3)-Co(2)	117.0(3)				
Symmetry transformations used to generate equivalent atoms: #1 x+1/2,y+1/2,z; #2 -x+3/2,y+1/2,-z+1/2; #3 -x+2,y,-z+1/2; #4 -x+2,-y+2,-z; #5 -x+3/2,-y+3/2,-z; #6 x,-y+2,z-1/2.					

1•4H_2O					
Bond lengths					
Co(1)-O(1)	2.030(4)	Co(1)-O(2)	2.074(4)	Co(1)-N(2)#2	2.124(5)
Co(2)-O(1)	2.006(4)	Co(2)-O(3)	2.042(4)	Co(2)-O(1)#5	2.146(4)
Co(2)-N(3)#4	2.061(5)	Co(2)-N(1)#3	2.074(5)		
Bond angles					
O(1)-Co(1)-O(2)	93.63(16)	O(2)#1-Co(1)-O(2)	88.9(2)	O(1)#1-Co(1)-O(1)	168.3(2)
O(1)-Co(1)-O(2)#1	94.69(16)	O(2)-Co(1)-N(2)#3	85.17(17)	O(2)-Co(1)-N(2)#2	173.54(17)
O(1)-Co(1)-N(2)#2	84.32(16)	O(1)-Co(1)-N(2)#3	88.25(16)	N(2)#2-Co(1)-N(2)#3	100.9(3)
O(1)-Co(2)-O(1)#5	78.57(17)	O(1)-Co(2)-O(3)	101.88(16)	N(3)#4-Co(2)-O(1)#5	85.64(17)
O(3)-Co(2)-O(1)#5	177.19(16)	O(3)-Co(2)-N(1)#3	89.12(18)	N(1)#3-Co(2)-O(1)#5	88.08(17)
O(3)-Co(2)-N(3)#4	95.34(17)	O(1)-Co(2)-N(1)#3	93.61(17)	N(3)#4-Co(2)-N(1)#3	115.74(18)
O(1)-Co(2)-N(3)#4	146.17(17)	Co(2)-O(1)-Co(1)	108.34(17)	Co(2)-O(1)-Co(2)#5	101.43(17)
Co(1)-O(1)-Co(2)#5	116.20(18)				
Symmetry transformations used to generate equivalent atoms: #1 -x,y,-z+1/2 #2 x-1/2,y+1/2,z #3 -x+1/2,y+1/2,-z+1/2 #4 -x+1/2,-y+3/2,-z #5 -x,-y+2,-z.					

1•EtOH					
Bond lengths					
Co(1)-O(1)	2.049(3)	Co(1)-O(3)	2.074(3)	Co(1)-N(2)#2	2.146(3)
Co(2)-O(1)	2.007(3)	Co(2)-O(2)	2.030(3)	Co(2)-O(1)#5	2.183(3)
Co(2)-N(1)#4	2.061(3)	Co(2)-N(3)#3	2.072(3)		
Bond angles					
O(1)-Co(1)-O(1)#1	169.97(16)	O(1)-Co(1)-O(3)	93.54(11)	O(3)#1-Co(1)-O(3)	89.71(17)
O(1)-Co(1)-O(3)#1	93.57(11)	O(1)-Co(1)-N(2)#2	84.53(11)	N(2)#2-Co(1)-N(2)#3	99.28(19)
O(3)-Co(1)-N(2)#2	174.75(12)	O(1)-Co(1)-N(2)#3	88.98(11)	O(3)-Co(1)-N(2)#3	85.54(13)
O(1)-Co(2)-O(2)	101.62(11)	O(2)-Co(2)-N(1)#4	94.89(12)	N(1)#4-Co(2)-N(3)#3	118.20(13)
O(1)-Co(2)-N(1)#4	143.29(12)	O(1)-Co(2)-N(3)#3	94.42(11)	N(1)#4-Co(2)-O(1)#5	86.12(12)
O(1)-Co(2)-O(1)#5	78.52(11)	O(2)-Co(2)-N(3)#3	90.42(13)	N(3)#3-Co(2)-O(1)#5	87.51(12)
O(2)-Co(2)-O(1)#5	177.93(11)	Co(2)-O(1)-Co(2)#5	101.48(11)	Co(1)-O(1)-Co(2)#5	115.84(12)
Co(2)-O(1)-Co(1)	107.25(12)				
Symmetry transformations used to generate equivalent atoms: #1 -x+1,y,-z+1/2 #2 x-1/2,y+1/2,z #3 -x+3/2,y+1/2,-z+1/2 #4 -x+3/2,-y+1/2,-z #5 -x+1,-y+1,-z.					

Table S4. Hydrogen-bonding interactions in the title compounds.

D-H...A	D-H(Å)	H...A(Å)	D...A(Å)	<DHA(°)
2•2DMF				
O(3)-H(3W)...O(4)#1	0.849(18)	2.20(4)	2.887(11)	137(5)
O(3)-H(3W)...O(1)#2	0.849(18)	2.58(6)	3.061(8)	117(5)
Symmetry transformations used to generate equivalent atoms: #1 x,-y+2,z-1/2; #2 -x+3/2,y+1/2,-z+1/2.				
1•4H_2O				
O(1)-H(1)...O(4)#1	0.821(18)	2.48(5)	3.171(3)	141.8
Symmetry transformations used to generate equivalent atoms: #1 x-1, y, z-1.				
1•EtOH				
O(1)-H(1)...O(4)#1	0.843(18)	2.23(4)	2.792(11)	124(4)
Symmetry transformations used to generate equivalent atoms: #1 x,y,z-1.				

Geometry comparison

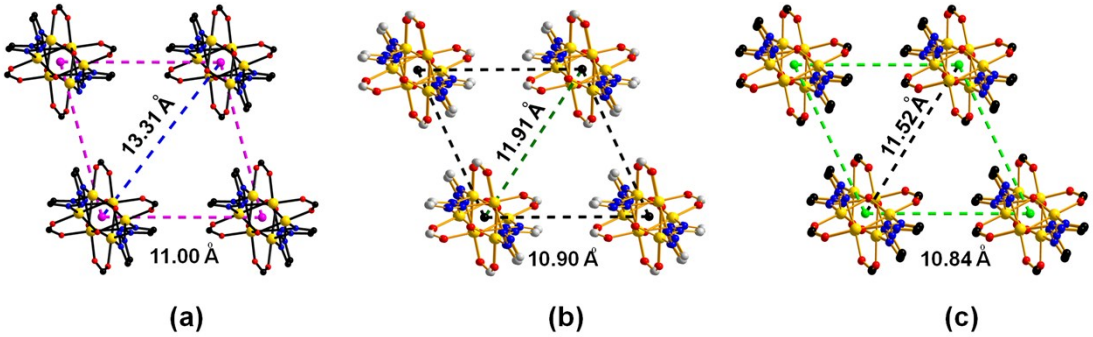

Fig. S27 The interchain distances comparison for **2·2DMF** (a), **1·EtOH** (b) and **1·4H$_2$O** (c).

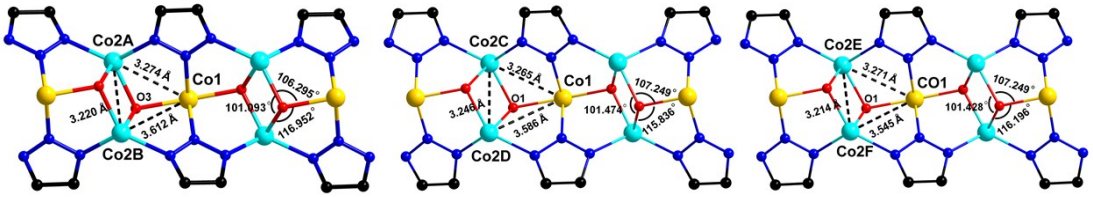

Fig. S28 The intrachain Co-Co distances and Co-O-Co bond angles comparison for **2·2DMF** (a), **1·EtOH** (b) and **1·4H$_2$O** (c).

Table S5. The geometry comparison for the title compounds.

	2•2DMF	**1•4H$_2$O**	**1•EtOH**
Co2—Co2[a] (Å)	3.220	3.214	3.246
Co1—Co2A (Å)	3.274	3.271	3.265
Co1—Co2B (Å)	3.612	3.545	3.586
Co1—Co1[a] (Å)	6.096	6.018	6.042
∠Co1—O—Co2A (°)	106.295	108.343	107.249
∠Co1—O—Co2B (°)	116.952	116.196	115.836
∠Co2A—O—Co2B (°)	101.093	101.428	101.474

[a] The shortest intrachain distance. A and B represent that the two Co2 ions bonded with the same μ_3-OH oxygen atom are located in two different symmetric positions. O represents the μ_3-OH oxygen atom.

Table S6. The free volume of the title compounds and their corresponding desolvated compounds calculated by the PLATON software.

Compound	**Free volume (Å^3)**	**Volume of per Unit Cell (Å^3)**	**Void ratio**
2•2DMF	89.9	2593.0	3.5%
2•2DMF [a]	1147.0	2593.0	44.2%
1•EtOH	245.8	2410.2	10.2%
1•EtOH [a]	938.7	2410.2	38.9%
1•4H$_2$O	309.8	2330.0	13.3%
1•4H$_2$O [a]	870.3	2330.0	37.4%

[a] The desolvated compounds of the title compounds.